Inelastic electron-hydrogen scattering in the unrestricted Glauber approximation*

J. N. Gau† and J. Macek
Behlen Laboratory of Physics, Unversity of Nebraska–Lincoln, Lincoln, Nebraska 68508
(Received 10 April 1975; revised manuscript received 7 July 1975)

The double-integral expression derived previously for Bryon's unrestricted Glauber approximation has been evaluated numerically to obtain scattering amplitudes for elastic collisions of electrons on hydrogen, as well as $2s$ and $2p$ excitation. The resulting values of cross sections and Ly-α polarization fractions are similar to previous Glauber calculations, but the alignment and orientation of Ly-α radiation as a function of scattering angle is markedly different from the predictions of the Born and conventional Glauber calculations.

I. INTRODUCTION

This paper is a presentation of results of numerical calculations using the double-integral expressions for electron-hydrogen scattering amplitudes derived in an earlier paper.[1] The expressions were derived using the Glauber approximation[2] without the usual assumption of purely transverse momentum transfer.

As discussed previously,[1] this assumption makes the scattering amplitude symmetric under reflection in the plane perpendicular to z, the direction of the path integral in the phase factor $\exp[(-i/\hbar v)\int_{-\infty}^{z} V\,dz']$ of Eq. (1) of Ref. 1. This symmetry permits excitation of only one substate[3] of the $2p$ level of hydrogen with the result that the Ly-α radiation is that of a single dipole whose electric vector lies in the scattering plane perpendicular to the direction z. Hence, choosing z perpendicular to the momentum transfer $\vec{q}$ forces agreement with the Born approximation, where the dipole is aligned with $\vec{q}$.[4]

Higher-order approximations whose transition operators have reflection symmetry only through the scattering plane allow excitation of two $2p$ substates with a relative phase difference. The purpose of this paper is to illustrate with numerical results some ramifications of these symmetry considerations.

The results presented in this paper were obtained from our two-dimensional integral expressions for electron-hydrogen scattering amplitudes in Byron's unrestricted Glauber approximation.[5] Section II reviews the expressions and their evaluation with details pertaining to numerical integration in the appendices. Section III contains results derived from numerical calculation of $1s \to 1s$, $1s \to 2s$, and $1s \to (2s+2p)$ scattering amplitudes. Differential cross sections from both the unrestricted and conventional Glauber versions for $1s \to (2s+2p)$ were plotted for comparison with the absolute measurements of Williams and Willis.[6] Also, we discuss the calculation of the orientation and alignment parameters[7] as applied to hydrogen Ly-α radiation detected in coincidence with the scattered electron. In addition to graphs of these parameters for various energies and scattering angles, we have included a plot comparing the measured linear polarization fraction with various calculations.

II. INTEGRAL EXPRESSIONS

In Ref. 1, Byron's six-integral expression

$$F(i \to f, \vec{q}) = \frac{-2m}{4\pi\hbar^2}\int e^{i\vec{q}\cdot\vec{R}} V(\vec{R},\vec{R}') \times \exp\left(\frac{-i}{\hbar v}\int_{-\infty}^{z} V\,dz\right) u_f^* u_i\, d\vec{R}\, d\vec{r}\,, \tag{1}$$

with

$$V(\vec{R},\vec{R}') = e^2(1/R' - 1/R)\,, \tag{2}$$

for electron-hydrogen scattering, was reduced to a two-integral expression. In Eqs. (1) and (2), $m\vec{v} = \hbar\vec{k}$ is the incident electron's momentum (which defines the z axis), $\vec{R}$ and $\vec{r}$ are the coordinates (relative to the nucleus) of the incident and bound electrons, respectively, $\vec{R}'$ is defined by $\vec{R}' = \vec{R} - \vec{r}$, the momentum transfer is defined by $\vec{q} = \vec{k} - \vec{k}'$, and u_i and u_f are the initial and final hydrogen bound states.

Since $u_f^* u_i$ is a product of polynomials and a factor $\exp[-\mu r + i(m_i - m_f)\phi]$, it can be expressed as a linear combination of terms generated by differentiating $\exp(-\mu r + i\vec{\gamma}\cdot\vec{r})$ with respect to μ and $\vec{\gamma}$.[8] Symbolizing this operation by $D(\mu,\vec{\gamma})$, we use $D(\mu,\vec{\gamma}) = 1$, $\mu = 2/a_0$, and $\vec{\gamma} = 0$ for $u_{1s}^* u_{1s}$. For $u_{2s}^* u_{1s}$ we apply $D(\mu,\vec{\gamma}) = 2 - a_0^{-1} d/d\mu$ and then set $\mu = 3/2a_0$ and $\vec{\gamma} = 0$.

By evaluating the integrals of Eq. (1) as far as possible before applying $D(\mu,\vec{\gamma})$, we obtained Eq. (17a) of Ref. 1, which is

$$F(i\to f,\vec{q})=\left[-2^{2-i\eta}\pi[\Gamma(-i\eta)]^{-1}\Gamma(1-i\eta)k\eta C_{fi}D(\mu,\vec{\gamma})4\mu\left(\frac{d}{d\mu^2}\right)^2\right]$$
$$\times\left(\int_0^\infty d\lambda\,\lambda^{-i\eta-1}\int_0^1 d\chi\,\chi^{-1}[\mathfrak{F}(1,0,0,0)-\mathfrak{F}(1,1,0,1)]\right), \tag{3a}$$

where

$$\mathfrak{F}(m,p,r,s)=\lambda^s(1-\chi)^s\Lambda^{-p}(\Lambda^2+q'^2)^{i\eta-m}(\Lambda-iq'_z)^{-i\eta-r}, \tag{3b}$$

$$\Lambda=[\lambda^2(1-\chi)^2+2i\lambda\chi(1-\chi)\gamma_z+\mu^2\chi+\gamma^2\chi(1-\chi)]^{1/2}, \tag{4a}$$

$$\vec{q}'=\vec{q}-i\lambda(1-\chi)\hat{z}+\chi\vec{\gamma}, \tag{4b}$$

C_{fi} is the appropriate normalization constant, $\eta=e^2/\hbar v$, and λ and χ are variables introduced by integral transformations.

The two remaining integrals in Eq. (3a) required numerical evaluation. Hence, it was necessary to first take the derivatives implied by $D(\mu,\vec{\gamma})\times 4\mu(d/d\mu^2)^2$. Because of the symmetry of the $1s\to 2p$ scattering amplitude and the properties of Y_{lm}, it was convenient to transform from a spherical to a Cartesian basis for the $2p$ hydrogen wave functions. In the coordinate frame of Fig. 1, we chose the basis defined by

$$u(2p_x)=-i\pi^{-1/2}(2a_0)^{-5/2}x\exp(-r/2a_0), \tag{5}$$

with similar expressions for $2p_y$ and $2p_z$. This choice means that $D(\mu,\vec{\gamma})=d/d\gamma_x$ for $F(1s\to 2p_x,\vec{q})$, $D(\mu,\vec{\gamma})=d/d\gamma_y$ for $F(1s\to 2p_y,\vec{q})$, and $D(\mu,\gamma)=d/d\gamma_z$ for $F(1s\to 2p_z,\vec{q})$. The numerical integration techniques for the scattering amplitudes and total cross sections are discussed in Appendices A and B, respectively.

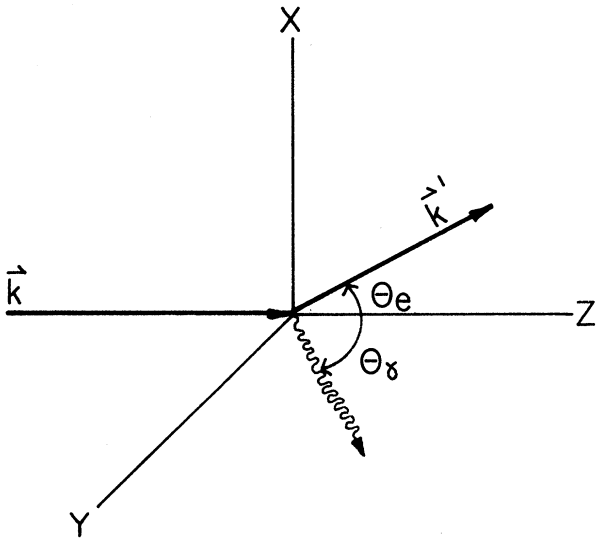

FIG. 1. Collision frame. The electron and photon detectors are positioned at angles θ_e and θ_γ, respectively, in the scattering x,z plane.

III. RESULTS

A. Cross sections

For fixed energy, the conventional Glauber $1s\to ns$ amplitudes diverge as $\ln q^2$ at small q and decrease as q^{-2} at large q, while the $1s\to np$ amplitudes diverge as q^{-1} at small q and decrease as q^{-3} at large q.[3] The unrestricted version is algebraically identical to the conventional expression of Ref. 3 at small q for elastic scattering and decreases as q^{-2} at large q for any state.

Hence, in Fig. 2 for 100- and 500-eV electrons

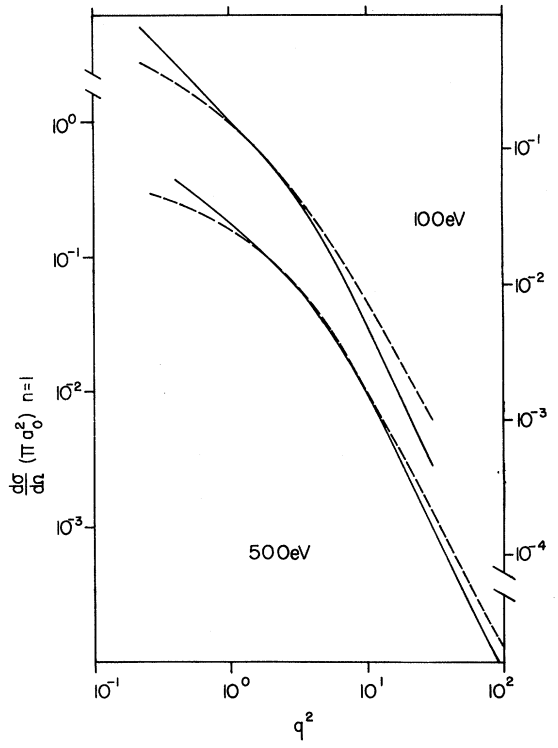

FIG. 2. Elastic differential cross section vs momentum transfer at 100 eV (in a.u.). The solid curve is our result while the dashed curve is that of Franco (Ref. 18).

scattering elastically from hydrogen, both versions should merge at small q and become parallel at sufficiently large q. The more rapid divergence of the unrestricted version as $q \to 0$ is the result of the nonconvergence of the numerical integrals as $q \to 0$.

Since $q^2 \sim (\Delta E)^2/2E$ for inelastic forward scattering, where ΔE is the energy loss, it is not surprising that our numerical integrals also converge poorly at 500 eV for angles less than 1°. Figure 3 shows this occurring for the 500-eV $1s \to 2s$ scattering amplitudes. For comparison, we calculated $1s \to 2s$ and $1s \to 2p$ conventional Glauber amplitudes from the equations of Ref. 3. Both conventional and unrestricted $2s$ amplitudes are similar at small q, but the conventional results are an order of magnitude larger at large q. However, as seen in Fig. 4, our total $2s$ cross sections agree with the conventional results of Ref. 9 and the unrestricted result of Ref. 5 except at 50 eV.

The relative behavior of the $2p$ Glauber amplitudes as a function of angle is typified by comparison with the recent 54.4-eV close-coupling result of Brandt and Truhlar.[10] Both 50-eV Glauber $2p$ cross sections are within 12% of the c.c. result for angles between 5 and 10°. At 0° the respective conventional and unrestricted values are 36% and 16% lower than the c.c. value, and at 180° they are 45% and 51% lower. The effect of the q^{-6}-vs-q^{-4} large-angle dependence of the conventional and unrestricted $2p$ cross sections is apparent at 500 eV where the conventional $2p$ result is less than 10% of the unrestricted $2p$ amplitude at angles greater than 90°. Figures 5–7 plot the absolute measurements and total error estimates of Williams and Willis[6] for comparison with the conventional and unrestricted Glauber $1s \to (2s + 2p)$ differential cross sections. Both versions agree with experiment at the smallest angles. As the angle increases, the conventional Glauber value remains closer to the experimental values, first because of the larger $2p$ amplitudes and later because of the large $2s$ amplitude. Neither version is very good at large q.

Figure 8 compares the total $1s \to 2p$ excitation-cross-section results of this paper with the unrestricted results of Ref. 5 and the conventional results of Ref. 9. The two unrestricted calculations are in agreement at all common energies and in agreement with the conventional result at those energies where Fig. 4 of Ref. 9 shows agreement of the conventional results with experiment.

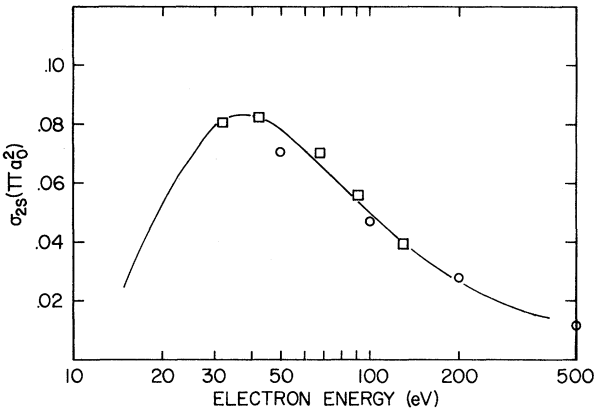

FIG. 4. Total $1s$–$2s$ cross section vs incident energy. The solid curve is the conventional Glauber result of Tai *et al.* (Ref. 9). The squares are the Monte Carlo results of Byron (Ref. 5). The circles are the results of this paper.

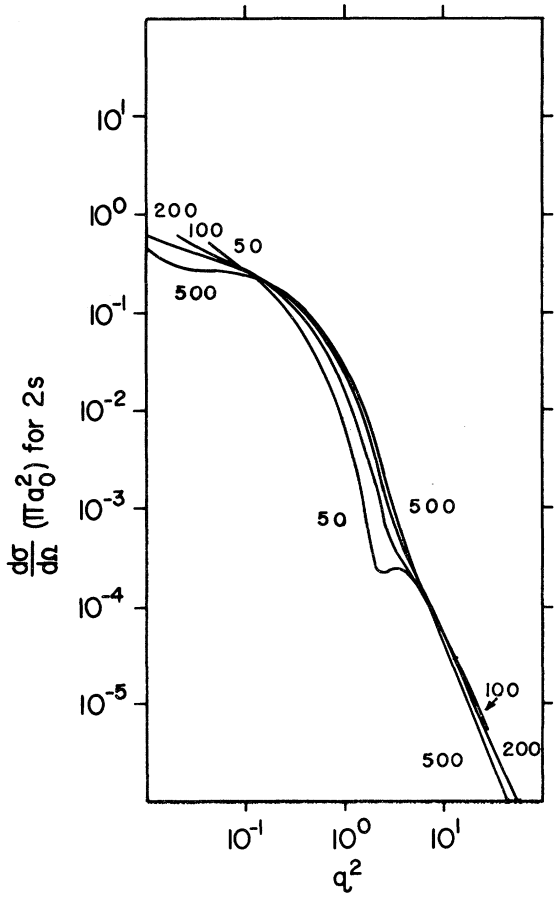

FIG. 3. $1s$–$2s$ differential cross section vs momentum transfer (in a.u.).

B. Orientation and alignment parameters

Recent experiments which detect radiation emitted by a collisionally excited atom in coincidence with the detection of a scattered particle enable one to deduce the relative phases as well as mag-

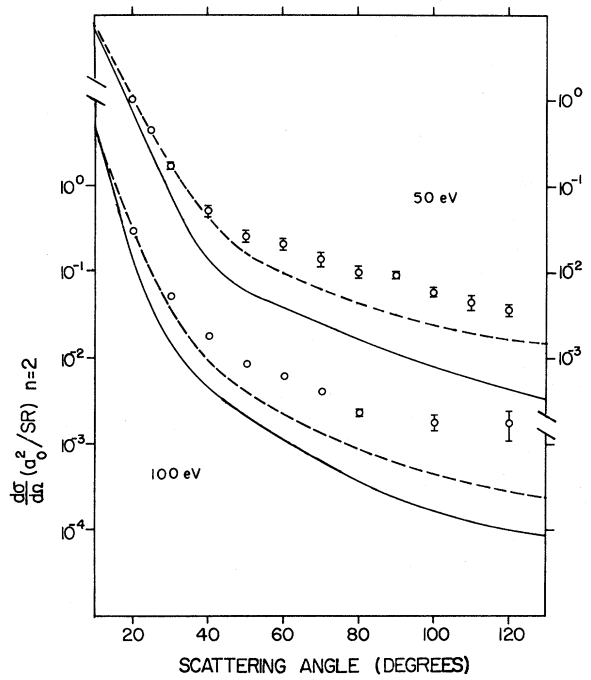

FIG. 5. $1s \rightarrow (2s+2p)$ differential cross section vs electron-scattering angle at 50 and 100 eV. Data points are those of Williams and Willis. The solid curves are the present calculation. The dashed curves were calculated using the conventional Glauber analytic expressions of Thomas and Gerjuoy (Ref. 3).

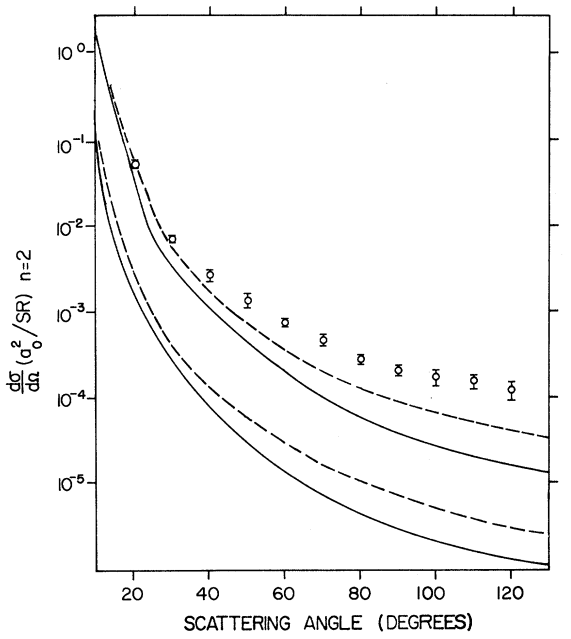

FIG. 6. Same as Fig. 5 for 200 and 500 eV. There were no measurements at 500 eV (lower curve).

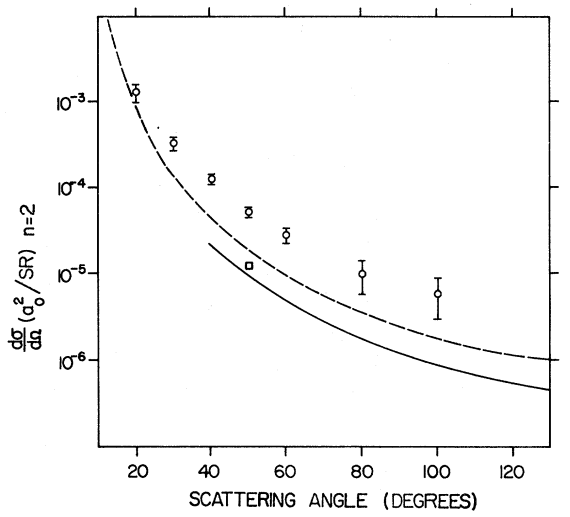

FIG. 7. Same as Fig. 5 for 680 eV. The solid curve includes only the dominant Rutherford terms. The □ is our calculation including all terms.

nitudes of complex excitation amplitudes for degenerate magnetic sublevels of the excited atom.[11] The relative phases depend on the dynamics of the scattering and the transfer of angular momentum to the atom; hence, their measurement provides a sensitive test of the qualitative correctness of scattering theories.

The predictions of the conventional and unrestricted Glauber approximations and the Born approximation will be discussed in terms of the Fano-Macek parameters,[7] which are components of tensors of rank 0, 1, and 2 constructed from the elements of $\vec{L}$. For electron-hydrogen scattering, where there is reflection symmetry about the scat-

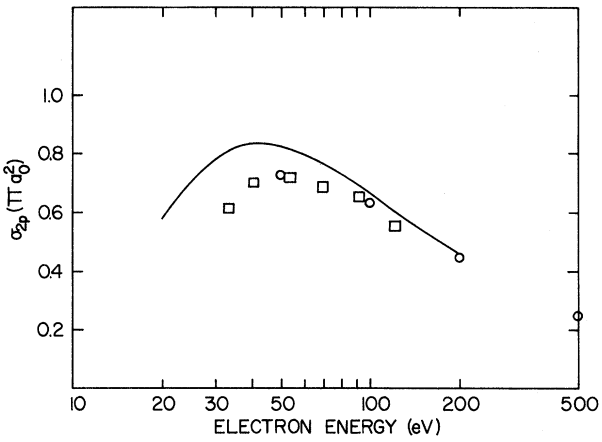

FIG. 8. As in Fig. 4 except for $1s$-$2p$ total cross section.

tering plane, the only nonzero parameters are given by Eq. (42) of Ref. 1. They are

$$O_{1-}^{\mathrm{col}} = \langle(\psi|L_y|\psi)\rangle/C\,, \tag{6a}$$

$$A_0^{\mathrm{col}} = \langle(\psi|3L_z^2 - L^2|\psi)\rangle/C\,, \tag{6b}$$

$$A_{1+}^{\mathrm{col}} = \langle(\psi|L_xL_z + L_zL_x|\psi)\rangle/C\,, \tag{6c}$$

$$A_{2+}^{\mathrm{col}} = \langle(\psi|L_x^2 - L_y^2|\psi)\rangle/C\,, \tag{6d}$$

where the superscript col refers to the collision frame whose coordinate system is chosen with $\hat{z}$ along $\hat{k}$, $\hat{y}$ along $\vec{k}\times\vec{k}'$, and $\hat{x}$ perpendicular to $\hat{z}$ and $\hat{y}$, as shown in Fig. 1, and $C = l(l+1)\sum|F_m|^2$ (l is the orbital-angular-momentum quantum number of the excited state). Using the basis defined by Eq. (5) for $1s \to 2p$, we obtain

$$|\psi) = F_{2p_x}|u_{2p_x}) + F_{2p_z}|u_{2p_z})\,, \tag{7}$$

observing $F_{2p_y} = 0$ because u_{2p_y} has odd parity under reflections in the scattering (x-z) plane. Substitution of Eq. (7) into Eq. (6) allows one to express the parameters explicitly in terms of the complex excitation amplitudes as

$$O_{1-}^{\mathrm{col}} = \frac{-\mathrm{Im}(F_{2p_x}^* F_{2p_z})}{|F_{2p_x}|^2 + |F_{2p_z}|^2}\,, \tag{8a}$$

$$A_0^{\mathrm{col}} = \frac{\frac{1}{2}|F_{2p_x}|^2 - |F_{2p_z}|^2}{|F_{2p_x}|^2 + |F_{2p_z}|^2}\,, \tag{8b}$$

$$A_{1+}^{\mathrm{col}} = \frac{-\mathrm{Re}(F_{2p_z}^* F_{2p_x})}{|F_{2p_x}|^2 + |F_{2p_z}|^2}\,, \tag{8c}$$

$$A_{2+}^{\mathrm{col}} = \frac{-\frac{1}{2}|F_{2p_x}|^2}{|F_{2p_x}|^2 + |F_{2p_z}|^2}\,. \tag{8d}$$

In the experiments of Eminyan *et al.*[11] for electron excitation of the He($2\,^1P$), the angular distribution of radiation in the scattering plane is measured by detecting the He($2\,^1P$-$1\,^1S$) decay photons emitted at polar angle θ_γ from the incident $\hat{z}$ direction in delayed coincidence with electrons scattered through the angle θ_e. The azimuthal angles Φ_γ and Φ_e of the photon and electron detectors are 0 and π, respectively, in the coordinate system of Fig. 1. The intensity of coincidence radiation is given by Eqs. (14) and (18) of Ref. 7:

$$I = \tfrac{1}{3}CS[1 - \tfrac{1}{2}h^{(2)}(j_i,j_f)A_0^{\mathrm{det}} + \tfrac{3}{2}h^{(2)}(j_i,j_f)A_{2+}^{\mathrm{det}}\cos2\beta + \tfrac{3}{2}h^{(1)}(j_i,j_f)O_0^{\mathrm{det}}\sin2\beta]\,, \tag{9a}$$

with

$$O_0^{\mathrm{det}} = O_{1-}^{\mathrm{col}}\sin\theta_\gamma\sin\varphi_\gamma\,, \tag{9b}$$

$$A_0^{\mathrm{det}} = A_0^{\mathrm{col}}\tfrac{1}{2}(3\cos^2\theta_\gamma - 1) + A_{1+}^{\mathrm{col}}\tfrac{3}{2}\sin2\theta_\gamma\cos\varphi_\gamma + A_{2+}^{\mathrm{col}}\tfrac{3}{2}\sin^2\theta_\gamma\cos2\varphi_\gamma\,, \tag{9c}$$

and

$$A_{2+}^{\mathrm{det}} = A_0^{\mathrm{col}}\tfrac{1}{2}\sin^2\theta_\gamma\cos2\psi_\gamma + A_{1+}^{\mathrm{col}}(\sin\theta_\gamma\sin\varphi_\gamma\sin2\psi + \sin\theta_\gamma\cos\theta_\gamma\cos\varphi_\gamma\cos2\psi)$$
$$+ A_{2+}^{\mathrm{col}}[\tfrac{1}{2}(1+\cos^2\theta_\gamma)\cos2\varphi_\gamma\cos2\psi_\gamma - \cos\theta_\gamma\sin2\varphi_\gamma\sin2\psi_\gamma]\,. \tag{9d}$$

(In this discussion, C and S remain undefined quantities which cancel out of the final equations.) When the photon detector is insensitive to polarization, Eqs. (9) must be averaged over the angles β and ψ, where β is defined by the elliptical polarization vector $\hat{\epsilon} \equiv (\cos\beta, i\sin\beta, 0)$ as discussed following Eq. (3) of Ref. 7, and ψ is the third Euler angle required to identify the orientation of a linear polarization analyzer. Because we are using eigenstates of orbital angular momentum $\vec{L}$, the coefficient $h^{(2)}(l_i,l_f)$ as defined by Eq. (8) of Ref. 7 is equal to -2 for $2p \to 1s$ transitions. So Eq. (9a) for this case becomes

$$I = \tfrac{1}{3}CS(1 + A_0^{\mathrm{det}})\,,$$

which, using Eq. (9c) and the definitions

$$\frac{F_{2p_x}}{F_{2p_z}} = \frac{|F_{2p_x}|}{|F_{2p_z}|}e^{i\chi} \tag{10a}$$

and

$$\lambda = |F_{2p_z}|^2(|F_{2p_z}|^2 + |F_{2p_x}|^2)^{-1}\,, \tag{10b}$$

becomes

$$I = \tfrac{1}{2}CS\{\lambda\sin^2\theta_\gamma + (1-\lambda)\cos^2\theta_\gamma$$
$$+ 2[\lambda(1-\lambda)]^{1/2}\cos\chi\sin\theta_\gamma\cos\theta_\gamma\}\,. \tag{10c}$$

Having determined λ and χ from Eq. (10), one can then determine the experimental values of the alignment and orientation parameters of Eq. (6) after expressing them explicitly in terms of λ and χ to obtain

$$O_{1-}^{\mathrm{col}} = [\lambda(1-\lambda)]^{1/2}\sin\chi\,, \tag{11a}$$

$$A_0^{\mathrm{col}} = \tfrac{1}{2}(1-3\lambda)\,, \tag{11b}$$

$$A_{1+}^{\mathrm{col}} = -[\lambda(1-\lambda)]^{1/2}\cos\chi\,, \tag{11c}$$

$$A_{2+}^{\mathrm{col}} = \tfrac{1}{2}(\lambda - 1)\,. \tag{11d}$$

Differentiating Eq. (10c) with respect to θ_γ, one finds that the minimum coincidence rate is obtained for the photon scattering angle given by

$$\tan 2\theta_{\min} = -2(2\lambda-1)^{-1}[\lambda(1-\lambda)]^{1/2}\cos\chi \quad (12a)$$

$$= 2A_{1+}^{\mathrm{col}}/(A_{2+}^{\mathrm{col}} - A_0^{\mathrm{col}}) \quad (12b)$$

$$= 2\,\mathrm{Re}(F_{2p_z}^* F_{2p_x})/(|F_{2p_x}|^2 - |F_{2p_z}|^2). \quad (12c)$$

When $\chi = 0$ as in the Born or conventional Glauber approximations, Eqs. (10) and (12) show that the minimum coincidence rate is zero when the photon detector is aligned parallel or antiparallel to the $\hat{z}$ or $\vec{q}$ direction in the Born approximation or the $\hat{x}$ axis in the conventional Glauber approximation. In both these approximations only a single magnetic substate is excited, and hence the radiation pattern is that of a single dipole oscillator. The Born approximation assumes very high incident energies where the interaction exciting the dipole can be considered instantaneous; hence, the dipole must be excited in the direction of recoil.

The conventional Glauber approximation can be made to give the same dependence of coincidence rate on angle by ad hoc redefining of the z direction as perpendicular to $\vec{q}$.[4] Then both the Born and conventional Glauber transition operators have reflection symmetry in the x,z and x,y planes. To see this explicitly, one can transform to the new (primed) coordinate frame defined by

$$z' = z\cos\theta + x\sin\theta, \quad (13a)$$

$$x' = -z\sin\theta + x\cos\theta, \quad (13b)$$

which implies

$$F'_{2p_z} = F_{2p_z}\cos\theta + F_{2p_x}\sin\theta \quad (14a)$$

and

$$F'_{2p_x} = -F_{2p_z}\sin\theta + F_{2p_x}\cos\theta. \quad (14b)$$

Hence the rotation $\theta = -\frac{1}{2}\pi$ transforms the single nonzero Glauber amplitude F_{2p_x} to $-F'_{2p_z}$ in the Born frame, where $\theta_{\min} = 0$. In the frame $\theta_{\min} = 0$, henceforth referred to as the major-axis frame, the Born and conventional Glauber orientation and alignment parameters defined by Eq. (8) are all zero except $A_0^{\mathrm{col}\prime} = -1$.

In contrast, in the unrestricted Glauber approximation, the parameters in the major-axis frame, obtained using Eqs. (8) and (14), are

$$O_{1-}^{\mathrm{col}} = -[\mathrm{Im}(F_{2p_x}^* F_{2p_z}]/\sigma, \quad (15a)$$

$$A_0^{\mathrm{col}\prime} = [|F_{2p_x}|^2(\cos 2\beta - \sin^2\beta) - |F_{2p_z}|^2(\cos 2\beta + \cos^2\beta) - 3\,\mathrm{Re}(F_{2p_x}^* F_{2p_z})\sin 2\beta]/\sigma, \quad (15b)$$

$$A_{2+}^{\mathrm{col}\prime} = -[|F_{2p_x}|^2\cos^2\theta_{\min} + |F_{2p_z}|^2\sin^2\theta_{\min} - \mathrm{Re}(F_{2p_x}^* F_{2p_z})\sin 2\theta_{\min}]/2\sigma, \quad (15c)$$

and

$$\sigma \equiv |F_{2p_x}|^2 + |F_{2p_z}|^2. \quad (15d)$$

[Equation (12b) shows $A_{1+}^{\mathrm{col}\prime} = 0$.]

A better physical understanding of the preceding discussion can be obtained by picturing the situation in the absence of spin with a semiclassical model.[12] Equation (12a) shows that the choice of the major-axis coordinate frame ensures $|\chi'| = 0$. The intensity of Ly-α radiation is then proportional to

$$|(u_{1s}|\hat{\epsilon}\cdot\vec{r}|\psi)|^2 = (\hat{\epsilon}\cdot\vec{d}_1)^2 + (\hat{\epsilon}\cdot\vec{d}_2)^2, \quad (16a)$$

where

$$\vec{d}_1 = (u_{1s}|x|u'_{2p_x})|F'_{2p_x}|\hat{x}',$$
$$\vec{d}_2 = (u_{1s}|z|u'_{2p_z})|F'_{2p_z}|\hat{z}'. \quad (16b)$$

This distribution is the average over one period of radiation from two classical oscillators $\vec{d}_1$ and $\vec{d}_2$ oriented along $\hat{x}'$ and $\hat{z}'$, respectively, oscillating 90° out of phase, and with magnitudes proportional to $|F'_{2p_x}|$ and $|F'_{2p_z}|$.

In an experiment where there is unresolved fine-structure splitting of the excited state, the radiation detected is that from a coherent superposition of states of slightly different energy. As discussed in Sec. III of Ref. 7, the resulting modulation of the intensity, anisotropy, and polarization of the emitted light requires multiplying the irreducible tensor components $T^{[k]}_q$ by the modulating factor $G^{(k)}(t)$, given by

$$G^{(k)}(t) = \sum_{j',j} \frac{(2j'+1)(2j+1)}{(2s+1)} \begin{Bmatrix} j' & j & k \\ l & l & s \end{Bmatrix}^2 \cos(\omega_{j'j}t), \quad (17)$$

where $\hbar\omega_{j'j} = E_{j'} - E_j$. The $T^{[k]}_q$ are formed from products of orbital-angular-momentum operators so that the $h^{(k)}(j_i,j_f)$ of Eq. (9a) become $h^{(k)}(l_i,l_f)$, where l_i and l_f are quantum numbers of orbital angular momentum. When the time resolution[11] of such coincidence experiments is no better than

the lifetime of the excited state, one must use the average $\langle G^{(k)}\rangle$, given by

$$\langle G^{(k)}\rangle = \frac{1}{\tau}\int_0^\infty G^{(k)}(t)e^{-t/\tau}dt\,. \tag{18}$$

Since $(\tau^2\omega_{j',j}^2+1)^{-1}\approx 0$ for $j'\neq j$, we obtain

$$\langle G^{(k)}\rangle = \sum_j \frac{(2j+1)^2}{(2s+1)}\begin{Bmatrix} j & j & k \\ l & l & s\end{Bmatrix}^2\,. \tag{19}$$

A coincidence experiment could, in principle, be done using a circular-polarization analyzer at $(\theta_\gamma=\pi/2,\ \phi_\gamma=\pi/2)$. The measured circular polarization P_c is then defined by

$$P_c = \frac{I_{\text{right}}-I_{\text{left}}}{I_{\text{right}}+I_{\text{left}}}\,. \tag{20}$$

Recalling the definition of β as used in Eq. (9a), we see that $\beta=\pi/4$ or $-\pi/4$ should be substituted into Eq. (9a) to obtain the intensities for right or left circularly polarized light, respectively. After substituting the resulting expressions from Eq. (9) into Eq. (20), we then obtain

$$P_c = 3O_0^{\text{det}}/(1+A_0^{\text{det}}) \tag{21a}$$

without spin, and

$$P_c = 3\langle G^{(1)}\rangle O_0^{\text{det}}/(1+\langle G^{(2)}\rangle A_0^{\text{det}}) \tag{21b}$$

with spin. From Eq. (18) we obtain[13] $\langle G^{(1)}\rangle=\frac{7}{9}$ and $\langle G^{(2)}\rangle=\frac{1}{3}$. Since $\theta_\gamma=\phi_\gamma=\pi/2$, Eq. (9b) reduces to

$$O_0^{\text{det}} = O_{1^-}^{\text{col}}\,. \tag{22}$$

It is easiest to evaluate A_0^{det} by quantizing about the detector axis. Then Eq. (11) of Ref. 7 becomes

$$A_0^{\text{det}} = \langle(\psi|\,3L_z^2-L^2\,|\psi)\rangle/2$$

which gives $A_0^{\text{det}}=\frac{1}{2}$, because $m_0=\pm 1$ owing to the reflection symmetry in the scattering plane. Hence, both Eq. (21a) and (21b) give $P_c=2O_{1^-}^{\text{col}}$ for this detector geometry (the result $P_c=\frac{42}{25}O_{1^-}^{\text{col}}$ of Ref. 1 was derived erroneously). This lack of depolarization from fine structure may be understood physically by noting that all photons detected by the analyzer in a dipole transition have unit angular momentum along the z axis. Hence, $\Delta m_j=\pm 1$ is the selection rule for any transitions seen by the photon detector on the z axis, just as $\Delta m_l=\pm 1$ is the selection rule without fine structure. The difference is that with fine structure some of the photons, namely those for which $\Delta m_j=0$, are emitted in other directions.

The parameters $\theta_{\min}$, λ, χ, $O_{1^-}^{\text{col}\prime}$, $A_0^{\text{col}\prime}$, and $A_{2^+}^{\text{col}\prime}$ were calculated after interpolating the real and imaginary parts of the numerically integrated amplitudes to obtain values at one-degree intervals.

In Fig. 9, we have chosen $\theta_{\min}$ so that in the Born approximation, $\theta_{\min}$ is the angle between $\vec{q}$ and

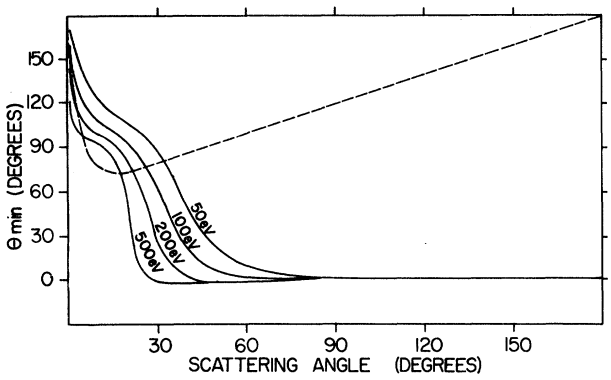

FIG. 9. Angle $\theta_{\min}$ vs electron scattering angle. The dashed curve is the Born result for 200 eV.

the negative $\hat{z}$ direction. The choice $\pi-\theta_{\min}$ would be equally valid as a solution of Eq. (12). For forward scattering the $\vec{q}$ and $\hat{z}$ directions are identical, so that both the Born and the unrestricted Glauber approximations predict only $2p_z$ excitation. The unrestricted Glauber $2p_x$ amplitude contains the factor $\sin\theta_e$ (θ_e is the electron scattering angle) which makes it identically zero for forward and backward scattering. At these two angles, the polarization ellipse becomes a straight line on the z axis, in agreement with the Born approximation.

Figure 10 shows the parameter λ, defined by Eq. (10b). Note that in the Born approximation Eq. (10b) becomes $\lambda=\cos^2\theta_{\min}$.

The phase χ plotted in Fig. 11 is the negative of the χ defined by Eq. (10a) so that negative χ in the plot corresponds to clockwise rotation of the electric vector as seen by a detector on the y axis (right circular polarization). In the major-axis frame, $|\chi|$ is always 90°, so that as the angle $\theta_{\min}$ between the major axis and the z direction approaches zero, $|\chi|$ approaches 90°.

Note in Fig. 12 that the circular polarization is

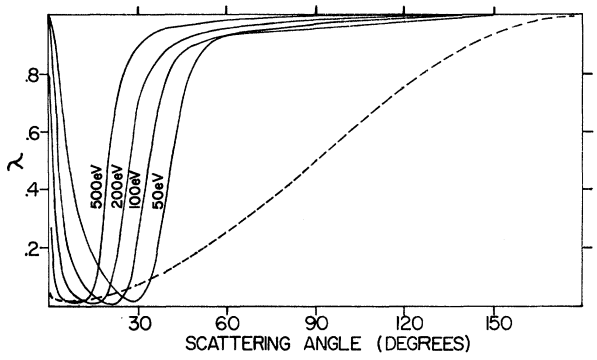

FIG. 10. Parameter $\lambda=\sigma_z/\sigma$ vs scattering angle. The dashed curve is the Born result at 500 eV.

always right except for at 50 eV. This may be understood crudely for small scattering angles by visualizing the atom as composed of two dipoles oriented along the axes of the polarization ellipse. We imagine each dipole to be excited at the instant when $\vec{R}$ is parallel to the axis of that dipole. The time lag between excitation of the first and second dipoles is comparable to the time of passage of the incident electron along its trajectory past the target. Hence for high incident energies the first dipole is excited to its maximum amplitude and is just beginning to decay when the second dipole is excited. Thus, the resultant dipole vector rotates clockwise. At a sufficiently low energy, however, the first dipole moment reaches its maximum negative value and starts back to zero as the second dipole is excited. Hence, the resultant dipole vector rotates counterclockwise. In this picture, the change from left to right circular polarization occurs when the time lag is half the period of the oscillators.

Figure 13 shows the two alignment parameters $A_0^{\mathrm{col}\prime}$ and $A_{2+}^{\mathrm{col}\prime}$ calculated in the major-axis frame where $\theta_{\min}$ and $A_{1+}^{\mathrm{col}\prime}$ are zero. In the major-axis frame, Eq. (8) shows that $A_0^{\mathrm{col}\prime}$ and $A_{2+}^{\mathrm{col}\prime}$ would be -1 and 0, respectively, in the Born approximation. Deviations from those values occur as the eccentricity of the polarization ellipse deviates from unity. Thus, one can specify the state of polarization completely (except for its sense, i.e., right or left) in terms of two parameters comparable to the orientation of the major axis and the eccentricity of the polarization ellipse. For example,

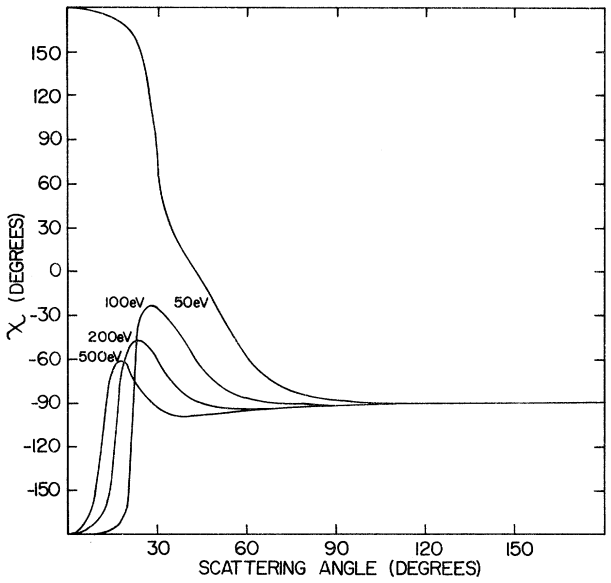

FIG. 11. Phase χ, defined as negative to that of Eq. (10a) of this paper.

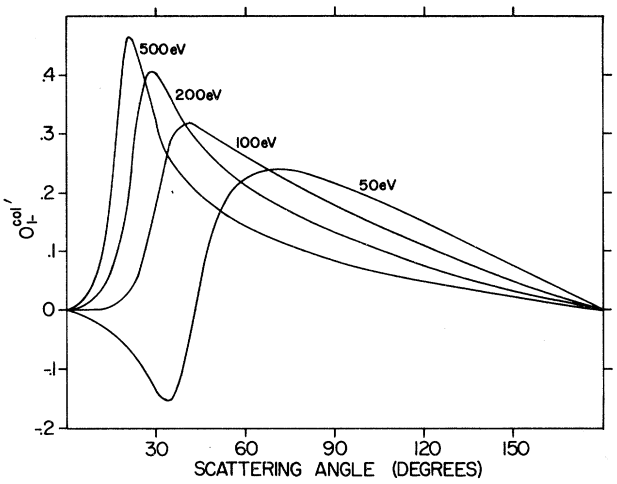

FIG. 12. Orientation $O_{1-}^{\mathrm{col}\prime}$ vs electron-scattering angle.

in the Poincaré sphere representation, the state of polarization is specified by the angular coordinates of a point on the sphere. In the experiments of Eminyan *et al.*,[11] the most convenient parameters were λ and χ.

C. Linear polarization fraction

Figure 14 compares the predictions of various calculations[4,5] with the experimental measurements of Ref. 14 of the polarization fraction P, defined

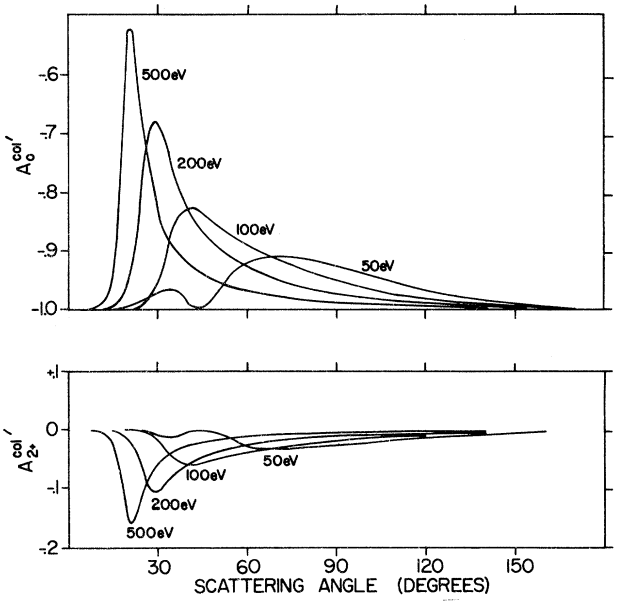

FIG. 13. Alignment parameters $A_0^{\mathrm{col}\prime}$ and $A_{2+}^{\mathrm{col}\prime}$ calculated in the "major-axis" frame where $\theta_{\min} = 0$. $A_{1+}^{\mathrm{col}\prime}$ is zero in this frame.

by

$$P=(I_{\parallel}-I_{\perp})/(I_{\parallel}+I_{\perp})\,, \tag{23}$$

where $I_{\parallel}$ and $I_{\perp}$ are the intensities of light polarized parallel and perpendicular to the $\hat{z}$ axis, averaged over all scattering angles. In terms of the Fano-Macek[7] parameters, Eq. (23) gives their Eq. (15):

$$P=\frac{3h^{(2)}(j_i,j_f)A_{2+}^{\det}}{2-h^{(2)}(j_i,j_f)A_0^{\det}}\,. \tag{24}$$

Including fine structure, Eq. (24) becomes the result of Percival and Seaton,[15] which is

$$P=\frac{3(2\sigma_z/\sigma_x-1)}{14\sigma_z/\sigma_x+11}\,. \tag{25}$$

In Eq. (25), σ_z and σ_x are the total cross sections for exciting the $2p_z$ and $2p_x$ states. Because the Born and conventional Glauber theories predict excitation of the same magnetic substate when the integration axis is redefined as done by Gerjuoy *et al.*,[4] any differences in P arise from the different shapes of the relative differential cross sections. The fairly close agreement of all the calculations of Fig. 14 shows that the polarization fraction is not very sensitive to differences in theories.

ACKNOWLEDGMENTS

We would like to thank Lester Lipsky for his suggestions for numerical integration and also William Campbell and Paul Finkler for useful discussions. We thank J. F. Williams for sending us his experimental results.

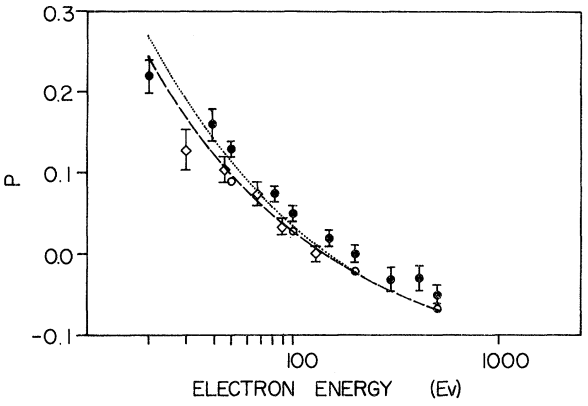

FIG. 14. Polarization fraction vs energy. The dashed line is the prediction of the Born approximation, the dotted line is the calculation of Gerjuoy *et al.* (Ref. 4), the diamonds are the Monte Carlo result of Byron (Ref. 5), the open circles are the present calculation, and the solid circles are the measurements of Williams and Willis (Ref. 6).

APPENDIX A: NUMERICAL INTEGRATION

Applying $D(\mu,\vec{\gamma})4\mu(d/d\mu^2)^2$ to Eq. (3) using Eq. (18) of Ref. 1 generates a sum of terms containing integrals of the form

$$I(g;h;m,p,r,s)=\int_0^{\infty}d\lambda\,\lambda^{-i\eta-1}\int_0^1 d\chi\,\chi^{g-1}(1-\chi)^h\mathfrak{F}(m,p,r,s)\,, \tag{A1}$$

where $g\geq 2$ is the total number of differentiations implied by $D(\mu,\vec{\gamma})4\mu(d/d\mu^2)^2$, and $h\geq 0$, $m\geq 1$, $p\geq s\geq 0$, $r\geq 0$ are the other integer exponents which parametrize the terms.

1. $1s\rightarrow 2p$

The integration for the $2p$ amplitude was performed using the Gauss product formula[16]

$$\int_{-1}^{1}dx\int_{-1}^{1}dy\,f(x,y)\simeq\sum_{i,j=1}^{n}A_i^{(n)}B_j^{(n)}f(x_i^{(n)},y_j^{(n)})\,, \tag{A2}$$

with x and y defined by

$$x=[\lambda(1-\chi)-1][\lambda(1-\chi)+1]^{-1}\,, \tag{A3a}$$

$$y=2\chi-1\,. \tag{A3b}$$

The integration points $x_i^{(n)}$ and $y_j^{(n)}$ are the zeros of the nth degree Legendre polynomials. The integrand $f(x,y)$ consisted of the sum of all the terms generated by differentiation.

2. $1s\rightarrow ns$

In order to discuss the solution to the convergence problems that occurred when evaluating Eq. (3a) for s states, it is necessary to recall and generalize results from Sec. III of Ref. 1, where we found an expansion of the integrand of Eq. (A1) in powers of μ/q. We also found an upper bound to the exact integral of Eq. (A1) which showed that in the case of $1s\rightarrow 2p$ scattering the dominant term at large q for fixed energy was $I(3;0;1,7,0,1)$, arising from the electron-nucleus interaction and having q^{-2} dependence. The generalization of Eq. (37) of Ref. 1 gives

$$|I(g;h;m,p,r,s)|\leq e^{2\pi\eta}\mu^{s-p}q^{-2m}q_z^{-r}(\tfrac{1}{2})B(\tfrac{1}{2}s,\tfrac{1}{2}(p-s))\,B(g+\tfrac{1}{2}(s-p),h+1)\,, \tag{A4}$$

which shows that the scattering amplitude for any excited state is dominated at large q by one or more q^{-2}-dependent terms arising from the electron-nucleus interaction.

For s states, these terms are not bounded by Eq. (A4) because $g+\frac{1}{2}(s-p)=0$. With the change of variables $t=\lambda(1-\chi)/(\mu\sqrt{\chi})$, which gives

$$I(g;h;m,p,r,s)=\mu^{-i\eta+s-p}\int_0^\infty dt\,t^{-i\eta-1+s}(1+t^2)^{-p/2}\int_0^1 d\chi\,\chi^{g-1+(s-p-i\eta)/2}(1-\chi)^{i\eta+h}(q^2-2iq_z\mu t\chi^{1/2}+\mu^2\chi)^{i\eta-m}$$
$$\times\{\mu\chi^{1/2}[(1+t^2)^{1/2}-t]-iq_z\}^{-i\eta-r}, \tag{A5}$$

we see that the integrand of these dominant terms is proportional to χ^{-1} as $\chi\to 0$. This divergence was removed using the asymptotic expansion of the integrand of Eq. (A1). To lowest order in μ/q, this consists of

$$(q^2-2iq_z\mu t\chi^{1/2}+\mu^2\chi)^{i\eta-m}\sim(q^2)^{i\eta-m} \tag{A6a}$$

and

$$\{\mu\chi^{1/2}[(1+t^2)^{1/2}-t]-iq_z\}^{-i\eta-r}\sim(-iq_z)^{-i\eta-r}, \tag{A6b}$$

which is also valid for arbitrary μ/q as $\chi\to 0$, which is substituted into the integrand of Eq. (A5). Calling the exact integrand $f(t,\chi)$ and the small-χ integrand $f_0(t,\chi)$, we then use the identity

$$\int_0^\infty dt\int_0^1 d\chi\,f(t,\chi)=\int_0^\infty dt\int_0^1 d\chi\,[f(t,\chi)-f_0(t,\chi)]+\int_0^\infty dt\int_0^1 d\chi\,f_0(t,\chi). \tag{A7}$$

The term $\int_0^\infty dt\int_0^1 d\chi\,f_0(t,\chi)$ was evaluated analytically using Eq. (32) of Ref. 1. To see if the first term of Eq. (A7) converges, one must examine the behavior of the second-order terms in the expansion of $f(t,\chi)$, since $f_0(t,\chi)$ is the first-order term in the expansion for large q or small χ. We obtain as $\chi\to 0$

$$f(g;h;m,p,r,s;t,\chi)-f_0(g;h;m,p,r,s;t,\chi)$$
$$\sim\{(i\eta-m)(-2iq_z)\,f_0(g;h;m+1,p,r,s+1;t,\chi)+(i\eta+r)[t(1+t^2)^{-1/2}-1]f_0(g;h;m,p-1,r+1,s;t,\chi)\}, \tag{A8a}$$

where

$$f_0(g;h;m,p,r,s;t,\chi)=q^{2i\eta-2m}(-iq_z)^{-i\eta-r}\mu^{-i\eta+s-p}t^{-i\eta-1+s}(1+t^2)^{-p/2}\,\chi^{g-1+(s-p-i\eta)/2}(1-\chi)^{i\eta+h}. \tag{A8b}$$

Inspection of Eq. (A8) shows that the difference integrand of Eq. (A7) for the s-state terms with $g+\frac{1}{2}(s-p)=0$ is proportional to $\chi^{-1/2}$ as $\chi\to 0$. This mild divergence can be removed from the summation in the Gauss formula

$$\int_a^b w(x)f(x)\,dx\approx\sum_{i=1}^n A_i^{(n)}f[x_i^{(n)}], \tag{A9}$$

by choosing the orthogonal polynomials defined by

$$\int_a^b w(x)P_n(x)P_m(x)\,dx=C_n\delta_{mn} \tag{A10}$$

so that the divergence is contained in the weight function $w(x)$. For Jacobi polynomials $P_n^{(\alpha,\beta)}(y)$, Eq. (A10) is

$$\int_{-1}^1(1-y)^\alpha(1+y)^\beta f(y)\,dy\approx\sum_{j=1}^n B_j^{(n)}f[y_j^{(n)}]. \tag{A11}$$

With the change of variables $y=2\chi-1$, the divergence $\chi^{-1/2}=(1+y)^{-1/2}$ is incorporated into the weight function by setting $\alpha=0$ and $\beta=-\frac{1}{2}$. With the additional change of variables $x=(t-1)(t+1)^{-1}$, we obtain the Gauss product formula

$$\int_{-1}^1 dx\int_{-1}^1 dy\,(1+y)^{-1/2}f(x,y)=\sum_{i,j=1}^n A_i^{(n)}B_j^{(n)}f[x_i^{(n)},y_j^{(n)}], \tag{A12}$$

where $f(x,y)$ is the original integrand times the factor $(1+y)^{1/2}$. The $A_i^{(n)}$ and $x_i^{(n)}$ are the weight coefficients and zeros for Legendre polynomials $P_n(x)$ and the $B_j^{(n)}$ and $y_j^{(n)}$ for Jacobi polynomials $P_n^{(0,-1/2)}(y)$.[17]

APPENDIX B: TOTAL CROSS SECTIONS AND RADIATION PARAMETERS

The Gauss quadrature formulas of the previous sections were used to obtain $F(1s\to 2s,\vec{q})$, $F(1s\to 2p_x,\vec{q})$, and $F(1s\to 2p_z,\vec{q})$ for $\theta=0$ to 180° at 10° intervals plus additional points needed for good interpolation using IBM scientific subroutines DATSM and DALI.

The interpolated values of $|F_{2s}|^2$ and $|F_{2p}|^2$ at 1° intervals were integrated numerically using the IBM subroutine DQSF (Simpson's rule and Newton's $\frac{3}{8}$ rule). The Glauber amplitudes peak sharply at $\theta=0°$ for high energies, while the total integrand drops sharply to zero at $\theta=0°$ because of the fac-

tor $\sin\theta$. Hence, the 1° interval was too coarse for Simpson's rule to work well near $\theta = 0°$ for 500-eV incident energy. In addition, the poor convergence of the Gauss quadratures at $\theta = 0°$ and 500 eV gave uncertain values of $2p_z$ and $2s$ amplitudes at that point, making interpolation uncertain for small angles. However, the Glauber $2p$ amplitudes approach the Born values as $q \to 0$. Thus, the total cross sections σ_{2p_x}, σ_{2p_z}, and σ_{2p} were recalculated using the Born amplitudes for the contribution from $0° \leq \theta \leq 1°$ at both 200 and 500 eV. The total cross sections are virtually unchanged at 200 eV and about 10% larger at 500 eV when this is done. The polarization fraction P of Eq. (25) is then in good agreement with other calculations.

The parameters $\theta_{\min}$, λ, χ, O_{1-}^{col}, A_0^{col}, and A_{2+}^{col} were calculated using interpolated values of both real and imaginary parts of the amplitudes $F(1s \to 2p_x \vec{q})$ and $F(1s \to 2p_z, \vec{q})$.

---

*Supported by National Science Foundation Grant No. GP-39310.

†Present address: Department of Physics and Astronomy, Louisiana State University, Baton Rouge, Louisiana 70803.

[1]J. N. Gau and J. Macek, Phys. Rev. A 10, 522 (1974).

[2]R. J. Glauber, in *Lectures in Theoretical Physics*, edited by W. E. Britten *et al.* (Interscience, New York, 1959), Vol. I., p. 315.

[3]B. K. Thomas and E. Gerjuoy, J. Math. Phys. 12, 1567 (1971).

[4]E. Gerjuoy, B. K. Thomas, and V. B. Sheorey, J. Phys. B 5, 321 (1972).

[5]F. W. Byron, Phys. Rev. A 4, 1907 (1971).

[6]J. F. Williams and B. A. Willis, J. Phys. B 8, 1641 (1975).

[7]U. Fano and J. Macek, Rev. Mod. Phys. 45, 553 (1973).

[8]For a discussion of this technique generalized to multielectron atoms, see the Comment of W. Williamson, Jr. and G. Foster in Phys. Rev. A 11, 1472 (1975).

[9]H. Tai, R. H. Bassel, E. Gerjuoy, and V. Franco, Phys. Rev. A 1, 1819 (1970).

[10]M. A. Brandt and D. G. Truhlar, Phys. Rev. A 11, 1340 (1975).

[11]M. Eminyan, K. B. MacAdam, J. Slevin, and H. Kleinpoppen, J. Phys. B 7, 1519 (1974).

[12]J. Macek and D. H. Jaecks, Phys. Rev. A 4, 2288 (1971).

[13]M. Rotenberg, R. Bivens, N. Metropolis, and J. K. Wooten, Jr., *The 3-j and 6-j Symbols* (Technology, Cambridge, Mass., 1959).

[14]W. R. Ott, W. E. Kauppila, and W. L. Fite, Phys. Rev. A 1, 1089 (1970).

[15]I. C. Percival and M. J. Seaton, Philos, Trans. R. Soc. Lon. A 251, 113 (1958).

[16]A. H. Stround and D. Seacrest, *Gaussian Quadrature Formulas* (Prentice-Hall, Englewood Cliffs, N. J., 1966).

[17]The $B_j^{(n)}$ and $Y_j^{(n)}$ were generated using the programs of Ref. 16, p. 28.

[18]V. Franco, Phys. Rev. Lett. 20, 209 (1968).